Article:

Day, H., Ingham, D. orcid.org/0000-0002-4633-0852, Ma, L. orcid.org/0000-0002-3731-8464 et al. (1 more author) (2021) Adjoint based optimisation for efficient VAWT blade aerodynamics using CFD. Journal of Wind Engineering and Industrial Aerodynamics, 208. 104431. ISSN 0167-6105

https://doi.org/10.1016/j.jweia.2020.104431

Adjoint based optimisation for efficient VAWT blade aerodynamics using CFD

Harry Day, Derek Ingham, Lin Ma, Mohamed Pourkashanian

Department of Mechanical Engineering, University of Sheffield

Corresponding author

Email address: Lin.Ma@sheffield.ac.uk

Postal address: Energy 2050, Ella Armitage Building, 40 Leavygreave Road, Department of Mechanical Engineering, University of Sheffield, Sheffield, S3 7RD

Abstract

The objective of this work is to demonstrate the viability of applying Adjoint methods to aerodynamic optimisation of VAWTs. Adjoint methods are very powerful optimisation techniques which have been implemented effectively in other fields, yet there is an absence of such work within VAWT literature.

A 'semi-transient' optimisation process is proposed, using Adjoint optimisation data from single instances in time to improve VAWT performance. This is challenging due to the unsteady nature of VAWT aerodynamics. A pitching aerofoil model approximates the VAWT flow field, drastically reducing computational cost. Details are given on the necessary CFD model(s), Adjoint solver settings, and optimisation philosophy.

The optimisation process was applied to a typical VAWT in the commercial CFD software ANSYS Fluent. A high tip-speed-ratio case is chosen to minimise unsteady flow affects. The results show novel blade geometries which improve the VAWT average power coefficient when compared to the original NACA0018 blade.

Such a method is novel in the field of VAWTs, and the use of Adjoint methods with low cost CFD models provides an efficient optimisation methodology that can be readily adopted by the VAWT design community. This work sets the foundation for a new and very promising avenue for VAWT research.

Keywords:
Adjoint
Aerodynamics
CFD
Optimisation
VAWT
Vertical Axis Wind Turbine

1 INTRODUCTION

Vertical Axis Wind Turbines (VAWTs) are comparatively underdeveloped compared to their Horizontal Axis Wind Turbine (HAWT) counterparts due to lack of research over the years (Bhutta *et al.,* 2011). VAWTs have some significant advantages over HAWTs and can be more useful in certain situations and conditions; for example in regions of unsteady winds and varying wind direction (Zhu *et al.,* 2015). They can be mechanically simpler with easier deployment and maintenance, and carry reduced demand on the support structure (Tjiu *et al.*, 2014). VAWTs should be explored further to pursue their full potential and improve the competitiveness of wind power in general. This would make it easier for investors, policy makers, and green thinking businesses to favour deployment of this renewable resource. In the future, VAWTs could play a very important role in offshore applications (Sutherland *et al.*, 2012), urban environments, and remote regions/micro-grids (Vassberg, et al., 2005).

The analysis and design of VAWT aerodynamics is more challenging than HAWTs due to difficulties in predicting the complex flow phenomena (Wang *et al.,* 2010). VAWT blades experience a constantly changing relative flow velocity, as well as a range of positive and negative Angles of Attack (AoA) over each revolution. At low Tip Speed Ratios (TSRs), dynamic stall is observed which comprises the complex formulation of vortices, followed by their development and separation into wakes (Wang *et al.,* 2010). Such time dependent flow physics have proven difficult to predict accurately making aerodynamic design and optimisation of VAWTs a significant challenge. Design methods for VAWT blades typically revolve around a set of conventional geometrical parameters (camber, thickness, fixing angle, solidity etc.) inherited from the field of aviation (Tjiu *et al.*, 2014).

While numerous authors have attempted to characterise the impact of these parameters on VAWT performance, geometry/performance trends are still not well understood over the full operating range (Edwards, 2012). Research to date is inconclusive in providing generalised trends for the effects of camber on VAWT performance. Some authors have claimed that introducing camber should be generally beneficial to VAWT power output such as Baker (1983) and Islam *et al.* (2007). Others find that camber can deteriorate the performance such as Worasinchai *et al.* (2016), calling symmetrical NACA sections a “simple and attractive choice for Darrieus rotors”. The appropriate camber is subject to the individual geometry and instantaneous operating conditions of each turbine.

Islam *et al.* (2007) states that a large blade thickness is beneficial at low TSR such as for self-starting, because thicker blades help delay stall at low Reynolds number.

Thickness is understood to be less desirable at higher TSR where separation issues become less prominent.

Fixing angle is the angle made between the blade chord and the blades tangential velocity (which is at right angles to the turbine connecting arm). Having a constant non-zero fixing angle causes a permanent skew to the range of AoA experienced by the blade. Klimas & Worstell (1981) investigated symmetrical aerofoils at different fixing angles and found small variations in fixing angle can exhibit great changes in the cut-in TSR, efficiency and peak power coefficient. Coton *et al.* (1996) states small non-zero fixing angles were found to reduce power output at low TSR but an improvement at high TSR, while large fixing angles were found to reduce the performance across all TSRs considered. At high TSR the AoA converges to the fixing angle, so the performance is more greatly influenced when the turbine is at operating speed (Hill *et al.,* 2008).

The solidity, σ, of a VAWT depends on the number of blades (N), blade chord (c) and rotor radius (R) and is defined as follows:

$$\sigma = \frac{\mathrm{Nc}}{\mathrm{R}} \tag{1.1}$$

Solidity has a strong effect on the performance of a VAWT. High solidity turbines operate more efficiently at low TSR and exhibit a sharp loss of efficiency away from the optimum. Low solidity turbines exhibit a smoother power curve, and experience maximum efficiency at higher TSRs (Edwards, 2012). Howell *et al.* (2009) experimented with solidity by varying the number of blades. It was found that the 3-bladed machine drastically outperformed the lower solidity 2-blade machine over the majority of the operating range considered.

Previous investigations into VAWT blade geometry parameters are useful but do not provide general performance trends over the full operating range (Edwards, 2012). Furthermore, designing VAWTs within these set of parameters is somewhat restrictive. Optimisation processes typically require large CFD (Computational Fluid Dynamics) campaigns in order to explore the variations of just a few parameters (Bianchini *et al.*, 2014). Therefore, efficient and powerful aerodynamic optimisation methods are desirable to aid more rapid development of VAWT technology.

VAWT optimisation in the literature tends to employ the Design of Experiments approach (Bianchini *et al.* 2014), whereby performance is evaluated after making semi-arbitrary changes to the blade geometry. This method is simple but is computationally inefficient and only a small number of design variables can be studied within a reasonable time frame. More refined forms of this method, namely Response Surface Methods (RSM) have been applied to VAWTs with success, but these also are lacking in efficiency as they disregard many poor system configurations during the process. RSMs also need to conduct an initial sampling stage of the solution space, which is akin to the design of experiments approach (Le Moigne, 2003).

An alternative form of optimisation method called genetic algorithms. These work by producing a multitude of semi-random design variations, and then eliminating those that perform poorly. The surviving designs are used to formulate the next range of test cases. These methods are also computationally wasteful due to many disregarded intermediary designs (Daróczy *et al.* 2018). None of these gradient-free methods mentioned so far use flow field data explicitly to determine the geometry change for the next iteration. On the other hand, gradient-based methods exist that calculate 'sensitivity gradients' from the flow field. These describe how the performance will vary for a given change in the blade geometry. Such sophisticated techniques therefore minimise computational wastage. Gradient-based methods have been developed for aerospace applications and hold great potential for VAWT technology.

Computing the sensitivity gradients directly can be very computationally expensive for problems with a large number of input variables, such as for an aerofoil. However, the Adjoint sensitivity analysis offers a unique advantage. Rather than performing additional sensitivity calculations for every input variable, the Adjoint variables are computed just once (per objective function) regardless of the number of input variables (Le Moigne, 2003). This Adjoint solution then provides the sensitivity gradients for all inputs which can be used in the gradient based optimisation process. For problems with many input variables this becomes an enormous benefit of Adjoint sensitivity analysis; the highly efficient computation of the sensitivity gradients produces a vastly more powerful gradient based optimisation process. As long as the number of objectives functions is less than the number of variables the Adjoint method is beneficial (Le Moigne, 2003). This is indeed the case for the problem of VAWT aerodynamics with a single objective function (of the moment coefficient or power coefficient), and complex blade geometries comprising hundreds of input variables in the form of nodal coordinates around the blade surface. It should be noted that other applications of Adjoint sensitivity analysis exist, but for the present work the combination of Adjoint sensitivity analysis along with gradient based optimisation will be referred to as 'Adjoint based optimisation'.

Using these methods a turbine blade can therefore be optimised in high resolution, rather than being constrained to a small number of shape parameters in order to limit computational cost. Adjoint based optimisation allows decoupling from the limitations of conventional aerofoil parameterisation, since the sensitivity gradients can be computed cheaply for every node; non-intuitive and unexpected solutions are possible.

Little research has been found in the literature on applying Adjoint methods specifically to wind turbine design problems although there has been some relating to HAWTs (Dhert *et al.,* 2016). The wider literature (mainly for aerospace) presents much in regard to Adjoint optimisation methods from a mathematical viewpoint, but not in direct application of Adjoint methods to the aerodynamic design problem of the VAWT.

The present work chooses to implement the Adjoint method for several reasons. Adjoints have not been used in conjunction with VAWTs in published research but they are potentially a very fruitful and exciting development in VAWT optimisation. Furthermore, popular CFD codes such as ANSYS Fluent have an Adjoint solver module, so that the methods developed here are widely accessible to the general CFD/VAWT community which increases the potential adoption and impact of this research.

One of the major obstacles of applying Adjoint methods to VAWTs is that their unsteady flow aerodynamics makes the use of transient Adjoint methods are extremely complex and time consuming, although some success has been shown in turbomachinery applications for transient Adjoints (Li *et al.,* 2011), (Walther & Nadarajah, 2015), (Luo *et al.,* 2011).

The current work constructs and presents an "engineering approach" which carefully applies a steady-state Adjoint solver to the transient problem of VAWT aerodynamics. This can be done despite the unsteady nature of the VAWT flow field. The focus of the paper is on the application of the Adjoint method rather than the complex inner workings of the mathematical formulation. There is a wealth of literature which the reader may consult for such insights, such as Errico (1997), Le Moigne (2003), Carpentieri (2009), and Coppin (2014).

This paper discusses the proposed methodology along with details of its application to a sample VAWT. This VAWT operates at a constant TSR of 4.5 and its performance is judged by the average power coefficient (C_P) achieved over a revolution. Larger scale VAWTs such as offshore turbines tend to have higher operating TSRs than small scale VAWTs, making a medium/high TSR VAWT a sensible choice for the present work (Worstell, 1978; Ashwill, 1992). Choosing a high TSR reduces the levels of flow unsteadiness as will be discussed in Section 2.1. An approximation model is used to reproduce the VAWT flow field via a single, isolated pitching blade. This significantly reduces computation cost, and details of this model are given in Section 2.1. 2D CFD simulations are used for the optimisation process and to quantify the performance of the baseline VAWT, which is validated against Rezaeiha *et al.* (Vol 107, 2017), and subsequently the VAWT fitted with candidate (optimised) blades. The validity of 2D vs 3D models for VAWT analysis is postulated by authors across the field and it is generally agreed that 2D analyses commonly overestimate the power coefficient (Howell *et al.,* 2009), (Almohammadi *et al.,* 2015) and (Jin *et al.,* 2014). This discrepancy is attributed to the spanwise flow components and over tip vortices which occur in reality and cannot be inferred by 2D simulations. Despite this, VAWT CFD research has predominantly consisted of 2D simulations using RANS turbulence models to alleviate high computational costs (Balduzzi *et al.,* 2015). The method described here could be extended to 3D simulations for greater accuracy (see planned future work in Section 5).

It is important to note that because the resulting optimised blade geometry is novel, no experimental data yet exists to provide additional validation of the CFD Results. However, validation of the CFD results is provided where appropriate.

2 METHODS

An Adjoint based optimisation method is developed in this paper which is illustrated using the widely known CFD code ANSYS Fluent. The method can however be reproduced and developed in other CFD codes that contain a steady Adjoint solver. As will be discussed, this method is described as ‘semi-transient Adjoint optimisation’ since it applies a steady Adjoint solver to unsteady aerodynamics problems.

A typical VAWT is used to illustrate the application of the method. This VAWT is as described in Rezaeiha *et al.* (Vol 107, 2017) with the turbine details presented in Table 1.

Turbine Blade Profile	NACA0018
Number of Blades	2
Blade Chord Length	0.06m
Blade Length	1m
Blade Fixing Angle	0 degrees
Turbine Diameter	1m
Rotational Velocity, ω	83.8 rad/s
Free-stream Wind Speed, U_{wind}	9.3 m/s
Tip Speed Ratio, λ	4.5

Table 1 - Details of the VAWT, Rezaeiha *et al*. (Vol 107, 2017).

This VAWT is selected due to its high TSR and due to the availability of data which can be used for CFD model validation. It should be noted that the CFD work of Rezaeiha *et al.* (Vol 107, 2017) is based on an experimental study conducted by Tescione *et al*. (2014). The following subsections describe the workings of the method.

2.1 Single-Blade Approximation CFD Model

To reduce computational cost of the optimisation process, a model with a single pitching blade is used to approximate the VAWT blade flow field. At the end of the optimisation, the resulting geometry is tested on a normal VAWT model (see Section 2.5). In this section, some VAWT theory is given followed by a description of the Single-Blade model which is based on this theory.

2.1.1 Turbine Blade Convention

The blades of a VAWT experience a flow velocity over a range of Angles of Attack (AoA) as the blades of the turbine revolve. Figure 1 shows the convention used for the aerodynamic force coefficients. The lift and drag force components produce a resultant force which has a blade normal component (C_N) and a tangential/chordwise component (C_T) which provides the useful torque:

$$C_T = C_L \sin(\propto) - C_D \cos(\propto) \quad (2.1)$$

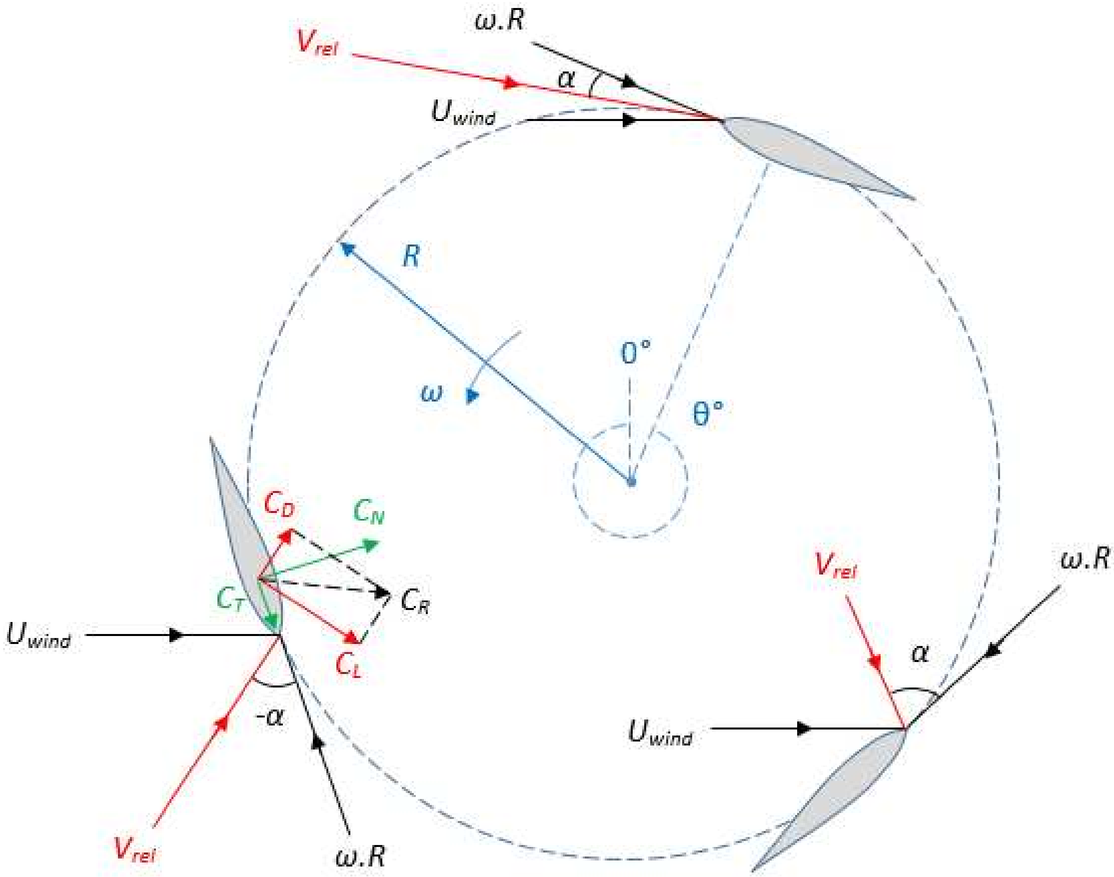

Figure 1 – Schematic of the Aerodynamic Coefficients of an Oscillating Aerofoil.

The TSR (λ) relates the wind speed and rotational velocity:

$$\lambda = \frac{\omega.R}{U_{wind}} \quad (2.2)$$

The relative flow velocity seen by a blade with zero fixing angle can be calculated in terms of the TSR (λ) and azimuthal angle of the blade θ (Ferrer & Montlaur, 2015):

$$V_{rel} = U_{wind}\sqrt{\lambda^2 + 2\lambda\, cos\theta + 1} \quad (2.3)$$

The corresponding angle of attack is defined as (Ferrer & Montlaur, 2015):

$$\tan \propto = \frac{\sin\theta}{\lambda + \cos\theta} \tag{2.4}$$

As the TSR increases, the AoA variation reduces and approaches the blade fixing angle. For the present work, a high TSR VAWT is used, which mitigates the severe flow unsteadiness associated with the dynamic stall phenomena at low TSR.

The terms moment coefficient (C_M) and power coefficient (C_P) are also introduced:

$$C_M = \frac{M_F}{\frac{1}{2}\rho \overline{V_{rel}}^2 S\, R} \tag{2.5}$$

Where M_F, is blade moment of force (N.m), S is area, R is turbine radius, $\overline{V_{rel}}$ is the average relative blade velocity (ω.R), and T is torque.

$$C_P = \frac{T.\omega}{\frac{1}{2}\rho {U_{wind}}^3 A} \tag{2.6}$$

2.1.2 Single-Blade Modelling Philosophy

The Adjoint based optimisation methodology uses a simplified CFD model to approximate the VAWT blade aerodynamics. This significantly reduces computation time and improves the stability/convergence of the Adjoint solver. This simplified model is a single, isolated aerofoil with an oscillating pitch (AoA). The AoA variation is similar to that experienced by the blades of a VAWT. A variable inlet velocity is applied to the Single-Blade model to emulate the blade relative velocity experience on a VAWT. These elements combined, produce a reasonable approximation to the VAWT blade flow field, although vortex/wake interactions and some plunging motion components are neglected (Wang *et al.,* 2010). The rotation axis is located at one quarter chord length from the leading edge.

To illustrate this, the link between the Single-Blade model and the VAWT, which it represents, is shown in Figure 2. V_{rel} is the relative velocity of the flow seen by the blade at location A. It should be noted that under the sign convention defined in Figure 1, the blade of Figure 2 shown in the upwind region has a negative AoA.

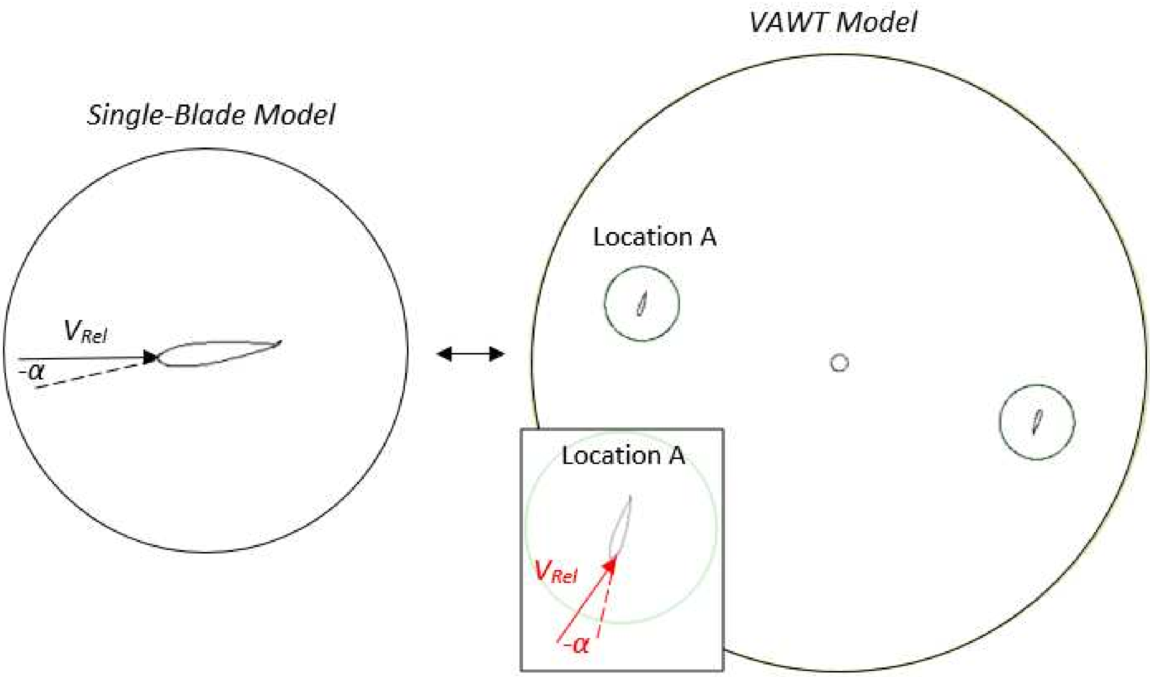

Figure 2 – AoA Similarity (link) Between the Single-Blade Model and the VAWT.

Figure 3 illustrates the agreement in the modelling results between a Single-Blade model and the VAWT which it represents (for the typical VAWT of Rezaeiha *et al*., Vol 107, 2017). As will be discussed later, the discrepancy in the downwind part does not affect the optimisation process, since the optimisation data used in this work is taken from the upwind part of the cycle only. This approximation model can therefore be of sufficient accuracy to replace a full VAWT model during the optimisation process. Due to the iterative nature of the process, this means significant computing time savings overall (Zhang *et al*., 2019).

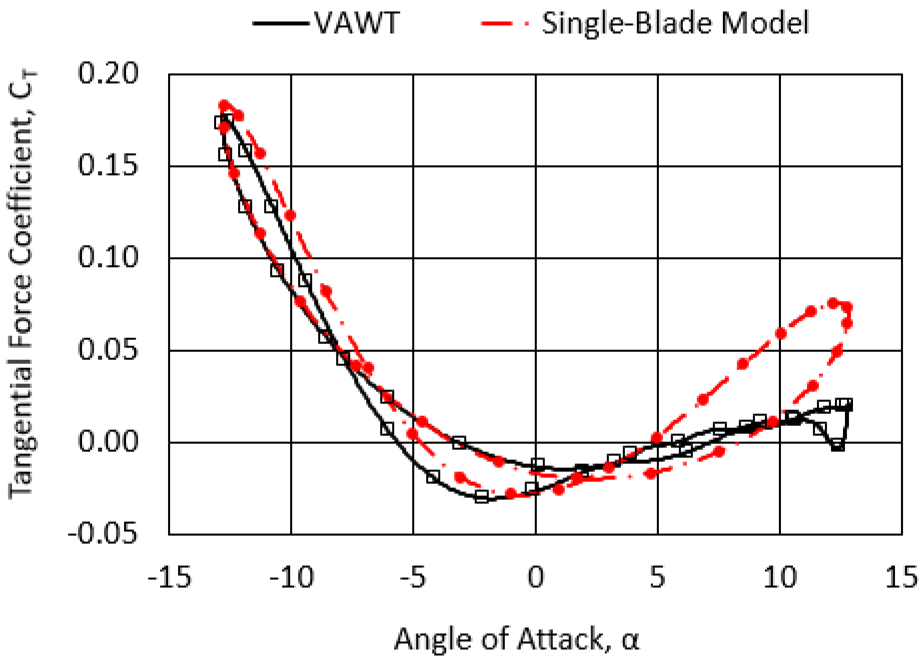

Figure 3 – Comparison of the Single-Blade Model Data and the VAWT Model Data.

2.1.3 Single-Blade Model CFD Setup/Validation

The sliding mesh technique was used with a User Defined Function (UDF) to provide the Single-Blade CFD model with the VAWT theoretical AoA profile, Equation (2.4). This technique consists of a circular non-conformal interface between the exterior mesh and the rotating subdomain, where mass/momentum exchange takes place. This practice is common within the literature Hand *et al.,* 2017. To more accurately represent the VAWT flow field, a knockdown factor of 0.5 was applied to the AoA in the downwind part of the cycle to account for transverse velocity components arising from energy extraction in the upwind and associated slow-down of the flow across the rotor (Gosselin *et al., 2013*). Variation in the blade relative velocity at the inlet is also prescribed via a UDF as per Equation (2.3).

The SST k-ω turbulence model is used for all the CFD simulations. Numerous authors have conducted investigations of turbulence model suitability for VAWTS using CFD and experimental data. Many authors deem that the basic 2 equation models, standard k-ε and standard k-ω incapable of predicting VAWT flows, while the SST k-ω variant is favoured over other models of similar complexity/cost and can adequately reproduce the VAWT flow fields (Wang *et al*., 2010), (Balduzzi *et al.,* 2015), (Hand *et al.,* 2017). Rezaiha *et al*. (2019) conducted a comprehensive study of the Spalart-Allmaras (S-A), RNG k-ε, realizable k-ε, k-ω SST, k-ω SST with intermittency, k-k_l-ω, and Transitional SST. A range of flow conditions were studied, with the conclusion that the SST models can provide reasonable predictions of VAWT flows including dynamic stall.

Although other high fidelity models, such as the k-ω SST with intermittency, Transition SST and even LES (Large Eddy Simulation) are recommended for better accuracy in transitional flows, the SST k-ω model is used in the present work. This is due to accuracy/cost considerations keeping in mind that the method here is presented in a basic form for demonstrating the feasibility. SST k-ω models are the most accurate type supported by ANSYS Fluent's Adjoint module that are also deemed suitable for VAWTs across the literature. In addition, for the high TSR case adopted here, it is judged that this turbulence model will be satisfactory as dynamic stall effects are minimal. The method presented can also be implemented in alternative open source CFD codes if Adjoint calculations using high fidelity turbulence models are required.

In the CFD simulations a value of 5% is used for the turbulence intensity, in accordance with the research paper of the VAWT (Rezaeiha *et al.,* Vol 107, 2017). The turbulence length scale, in lieu of specified values, is set as the turbine diameter (Rezaeiha *et al.* Vol 156, 2018).

For the Single-Blade CFD model (VAWT approximation model), the adopted domain and meshing strategy is close to that used in Hand *et al.* (2017), utilising a circular far-field zone and circular subdomain. This makes producing a high quality structured mesh easier, with the ability to make rapid amendments and refinements. A near-wall refined zone allows a first cell thickness to achieve a y+ of approximately 1 which is sufficiently small to resolve the viscous sublayer without the necessity of a wall function (Wang *et al.,* 2010).

The CFD simulations are solved using the Coupled Numerical Scheme. The pressure based solver is used with the second-order upwind scheme for spatial discretisation, and the bounded second-order implicit scheme for the transient formulation. A limit of 30 iterations per time step is used and minimum convergence criteria of $1\text{x}10^{-5}$ is set for all residuals. These settings are common across the VAWT CFD literature in order to achieve sufficient solution convergence (Li et al., 2018, Wang et al., 2010, Rezaeiha et al., Vol 107, 2017, and Guo et al., 2019).

To validate the Single-Blade model, grid, and time-step independence studies were performed for a constant domain size. The range of meshes and time-steps are presented in Table 2 and 3, respectively.

Mesh I.D.	**M1**	M2	M3	M4	M5
Total cells (k = 1000 cells)	**54 k**	102 k	150 k	245 k	345 k
Num. cells around aerofoil surface	**310**	380	475	570	680

Table 2 - Range of Meshes Used in the Validation Study.

Time Step I.D.	T1	T2	T3	**T4**	T5	T6	T7
Num. steps per turbine revolution	100	200	400	**800**	1200	1600	2000

Table 3 – Range of Time-Steps Used in the Validation Study.

Over the range of time-steps studied the medium-fine time-steps (T4, T5) showed near perfect agreement with each other, and closely matched the finest time-steps (T6, T7). Taking consideration of required accuracy and computation costs of the optimisation process, time-step T4 (800 time-steps/rev) was deemed suitable. In a similar fashion, the range of meshes were tested at the chosen time-step (T4). The finest mesh had near perfect agreement with the coarsest mesh, along with the other cases in between but has around 7 times the number of cells It was concluded that the coarsest mesh (M1) is suitable. A range of domain sizes were then tested for a constant mesh density (see Table 4).

Domain I.D.	D1	D2	**D3**	D4	D5
Total cells (k = 1000 cells)	33 k	43 k	**54 k**	64 k	73 k
Diameter of rotating subdomain (as a multiple of chord length)	2c	4c	**6c**	8c	10c
Diameter of far-field zone (as a multiple of chord length)	15c	25c	**40c**	65c	100c

Table 4 – Range of domains used in the validation study.

There was relatively close agreement across all the domain sizes. Only minor disagreements were observed between D3, D4 and D5, and considering that D4 and D5 have 19% and 37% more cells compared to D3, respectively, it was judged that D3 is the most appropriate domain size to use

Having demonstrated mesh, time-step and domain size convergence of the solution, it is then necessary to check the flow field of the Single-Blade model against the VAWT blade flow field. To allow a direct comparison (see Figure 3), the VAWT blade moment data is converted to C_T and the theoretical AoA is determined according to Equation (2.4). In a similar fashion, the Single-Blade data is converted to a theoretical C_M as a function of the azimuthal angle curve, allowing this comparison to be viewed in a more typical VAWT format (see Figure 4).

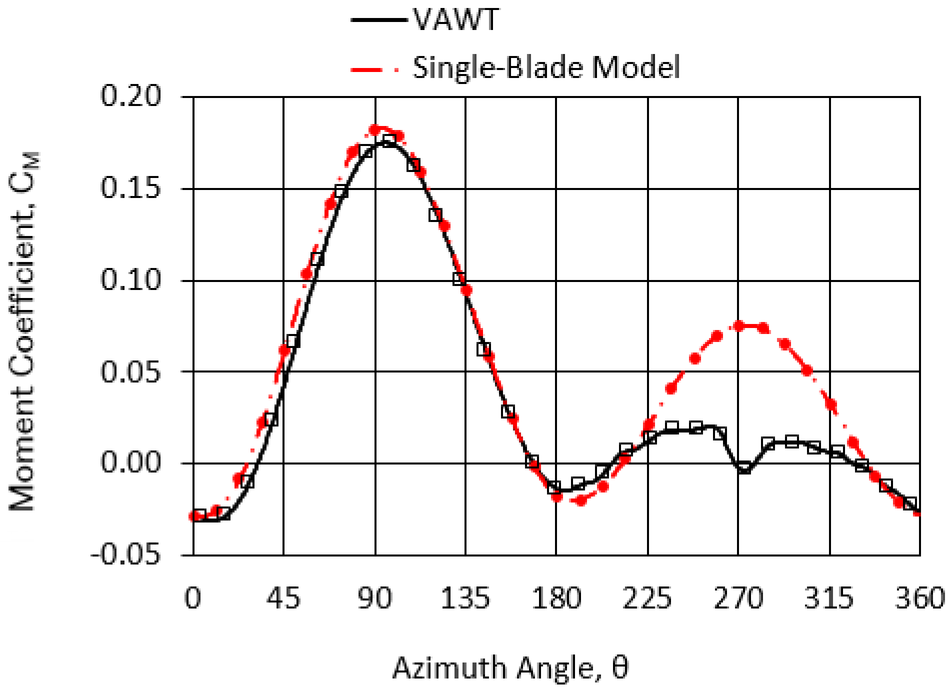

Figure 4 – Comparison of Single-Blade Model Data and VAWT Model Data (C_M).

Figure 3 and Figure 4 show that the Single-Blade model is successful in providing an approximate flow field of the VAWT blades, although the representation in the downwind part of the cycle is somewhat inaccurate. The inaccuracies are due to neglecting the blockage effects and shaft/blade wake interactions in the downwind region. However, this is not detrimental to the optimisation method since sensitivity data is taken only from the upwind part in the present work. The Single-Blade model is therefore a suitable approximation to use in the optimisation process. The new aerofoil derived from the optimisation process will be further validated through a full turbine simulation.

2.2 Philosophy of the Semi-Transient Optimisation

As described in Section 2.1, the Single-Blade model provides a platform upon which the Adjoint based optimisation can take place. The optimisation makes use of an Adjoint solver configured for steady-state flows. Steady Adjoint solutions *can* however be of value and of use for engineering approaches for unsteady problems (Eggenspieler, 2012). The method/optimisation process developed here is such an engineering approach for the transient problem of VAWT aerodynamics. Further details of the process are presented in Section 2.4.

2.2.1 Objective

Any optimisation process aims to produce a solution that approaches the extrema of a given objective function. With regard to VAWTs, one can generally assume that the objective is to maximise the average power coefficient, but since this quantity does not depend on an instantaneous flow field, the tangential blade force coefficient (C_T) is selected (see Figure 1). A blade geometry once optimised for C_T in the Single-Blade model, will give higher power output when placed on a VAWT. The sensitivity gradients (described in Section 1) resulting from the Adjoint solver in this case describe the change in C_T that would arise from a given change to the blade geometry.

2.2.2 Snapshots

Despite the unsteadiness of VAWT aerodynamics, a steady Adjoint solver can be applied to an instantaneous snapshot of the transient flow field. A snapshot corresponds to a single point in time, when the aerofoil is at a given angle during its oscillation cycle. The overall optimisation can thus be considered to be a 'semi-transient' method – the flow field solution arises from a fully transient CFD simulation, but the Adjoint solutions are limited to consider data from one (or several individual) instance in time.

Figure 5 shows the baseline Single-Blade performance curve, with the position of an arbitrary snapshot marked in terms of AoA. The example snapshot shown in this case is taken during the upwind part of the cycle as the negative AoA is increasing towards its extrema. The arrows indicate the direction of the pitching motion.

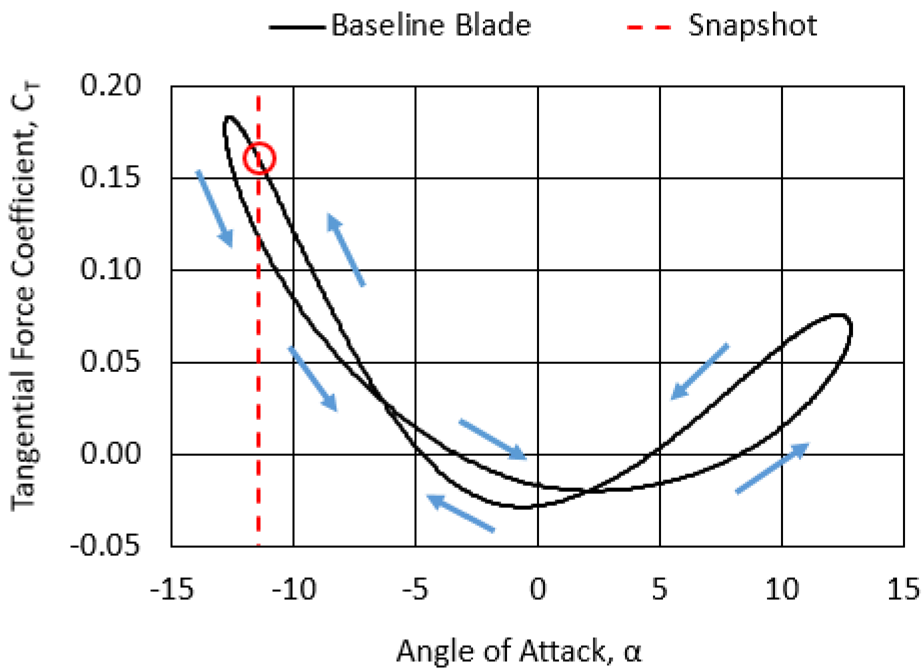

Figure 5 – Single Blade Performance Curve with the Snapshot Location Marked.

The successful application of the semi-transient method hinges on the choices of the AoA for which the flow field snapshot(s) are taken. The snapshot(s) used could be located at any point during the cycle. The present work considers the use of just 1 snapshot for each cycle of the blades oscillation. To investigate the effects of snapshot location on the outcome of the Adjoint based optimisation process, a range of 1-snapshot cases were tested, with each one corresponding to a snapshot position 30 degrees greater than the previous case. Although the snapshot choice is a fundamental element of the semi-transient method, the results of this investigation are deferred to Section 3 so that other details of the method can first be discussed.

2.3 Adjoint Module Setup

The present work employed the Adjoint solver in ANSYS Fluent which has a range of settings which should be configured in order for this optimisation process to operate successfully. Very little guidance exists in the literature on what Adjoint module settings to use, and so for the current work the values/choices made have been derived mainly from preliminary studies.

Table 5 shows a summary of the settings in the ANSYS Fluent Adjoint module, the discussion of which is provided in the following sub sections.

Objective function:	Tangential blade force coefficient (C_T)
Target performance change:	+3% (of the objective function)
Adjoint solution iteration limit	1000 iterations
Adjoint solution stability scheme	Automatic
Geometric constraint	Constant chord length
Size of mesh morphing zone as a multiple of chord length	1.8c (x), 1.1c (y)
Number of control points in mesh morphing zone	100 (x), 100 (y)
Freeform Scaling Scheme	Objective reference change
Freeform Scale Factor	1

Table 5 – Adjoint Module Settings Summary.

2.3.1 Solver settings

A limit of 1000 iterations is applied for when the Adjoint solution is calculated. This offers a balance between solution convergence, and computational cost. The convergence criteria values for the Adjoint equations are set as the default values. Stabilisation scheme options are offered for the Adjoint solver when the standard advancement scheme is unstable. The current work uses the ‘auto-assign’ option which chooses the most appropriate scheme automatically if numerical divergence is detected during the calculation of the Adjoint solution. The Adjoint solutions have generally reached convergence well within the 1000 iteration limit, and thus do not require stabilisation.

The Adjoint solution, once obtained, merely provides the gradient of the objective function (C_T) with respect to the input variables (blade geometry). This in itself is not the solution to the aerodynamic design problem, and these sensitivity gradients are used later to perform mesh morphing to produce an improved geometry.

2.3.2 Objective Target

The target of performance/objective improvement can be specified by the user, acting as a level of aggression in the optimisation process. In the present work a target of + 3% in the value of C_T is used. The mesh morpher attempts to implement this target by scaling the projected geometry changes of the blade.

2.3.3 Geometry Constraints & Mesh Morphing Settings

Before applying mesh morphing to the blade geometry, constraints can be specified which limit the deformation. To give the VAWT optimisation process a more real-world applicability, constraints should be involved that represent requirements from other engineering disciplines outside those of pure aerodynamics. For the present work where the focus is aerodynamic optimisation, the constraints have been approached simply with just a chord constraint being implemented. A chord change would alter the turbine solidity. To avoid this kind of ‘false’ optimisation, the optimisation process should operate at a constant solidity (chord) in order to produce a valuable outcome. A constant fixing angle is *not* imposed as a constraint as this could restrict performance improvements unnecessarily; the optimisation can provide the optimum fixing value implicitly after the geometry changes have been made.

To implement a chord constraint whist allowing freedom of the fixing angle and other geometry changes, a circular boundary is used. This boundary envelopes the blade as shown in Figure 6 (a). Consideration must be given to whether the constraint is designated as “strict” or not. Preliminary studies showed that using strict conditions can produce negative cell volumes after the morphing operation takes place. Using non-strict conditions alleviates this issue but permits some non-conformance at the constraint boundary (i.e. the blade geometry may partially enter the boundary). The degree of this non-conformance can be limited by using appropriate values for Free Form Scaling Factor, and Number of Control Points (see ANSYS user manual, ANSYS Help §35.2.5.5, 2017). The present work uses non-strict conditions. No geometrical parameterisation takes place or is required. The sensitivity gradients are computed on a node by node basis, and the mesh morphing is performed on a similar basis via the set of Control Points.

The user can also define the region of the mesh in which mesh morphing is permitted to occur. This relates to cells surrounding the blade which must move to accommodate the geometry changes of the blade wall. The region used in the present work surrounds the blade wall and no other features/boundaries/interfaces, see Figure 6 (b).

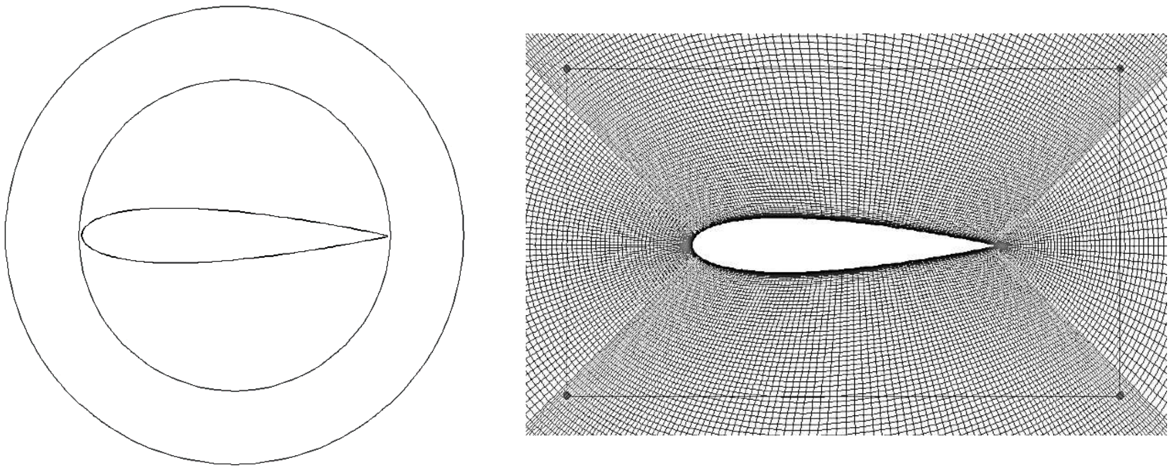

Figure 6 – (a) Constraint Boundary (Left) and (b) Mesh Morphing Zone (Right).

2.4 Optimisation Process

A concise general overview of the Adjoint optimisation procedure is given in Section 2.4.1 before a discussion is given on the semi-transient Adjoint based optimisation process developed here for VAWTs (Section 2.4.2),. The level of detail provided aligns with the ANSYS Fluent Adjoint module, but the process is similar for other CFD codes but more steps may be involved.

2.4.1 General Adjoint Optimisation

Figure 7 shows a flow chart of the Adjoint optimisation procedure in general terms.

The Adjoint solution requires a standard CFD flow field solution to have been computed (step 3). The flow field solution is used by the Adjoint solver to compute the sensitivity gradients at each node on the blade surface (step 4). These data describe how a deformation at each surface point effects the overall performance. As previously stated the performance or 'objective function' is specified by the user. An example set of sensitivity vectors can be seen in Figure 10.The mesh morpher determines an appropriate incremental change to each surface node position in the direction of improvement (step 7). The degree of movement here depends on the constraints, and 'aggression' settings within the mesh morphing tool, as well as the sensitivity data itself. With the updated geometry the standard flow field solution must be recomputed such that the performance can be re-evaluated. An optimisation process would typically be run for as many iterations as required to reach convergence of the objective function. In this work a candidate blades true performance cannot be known until a candidate VAWT is produced. To mitigate the need for constructing many candidate VAWT models for each case, preliminary studies were made to decide an appropriate number of iterations to run the single blade optimisation. 10 iterations were chosen and used in the present work, as this approximated the optimum number of iterations for the range of cases tested.

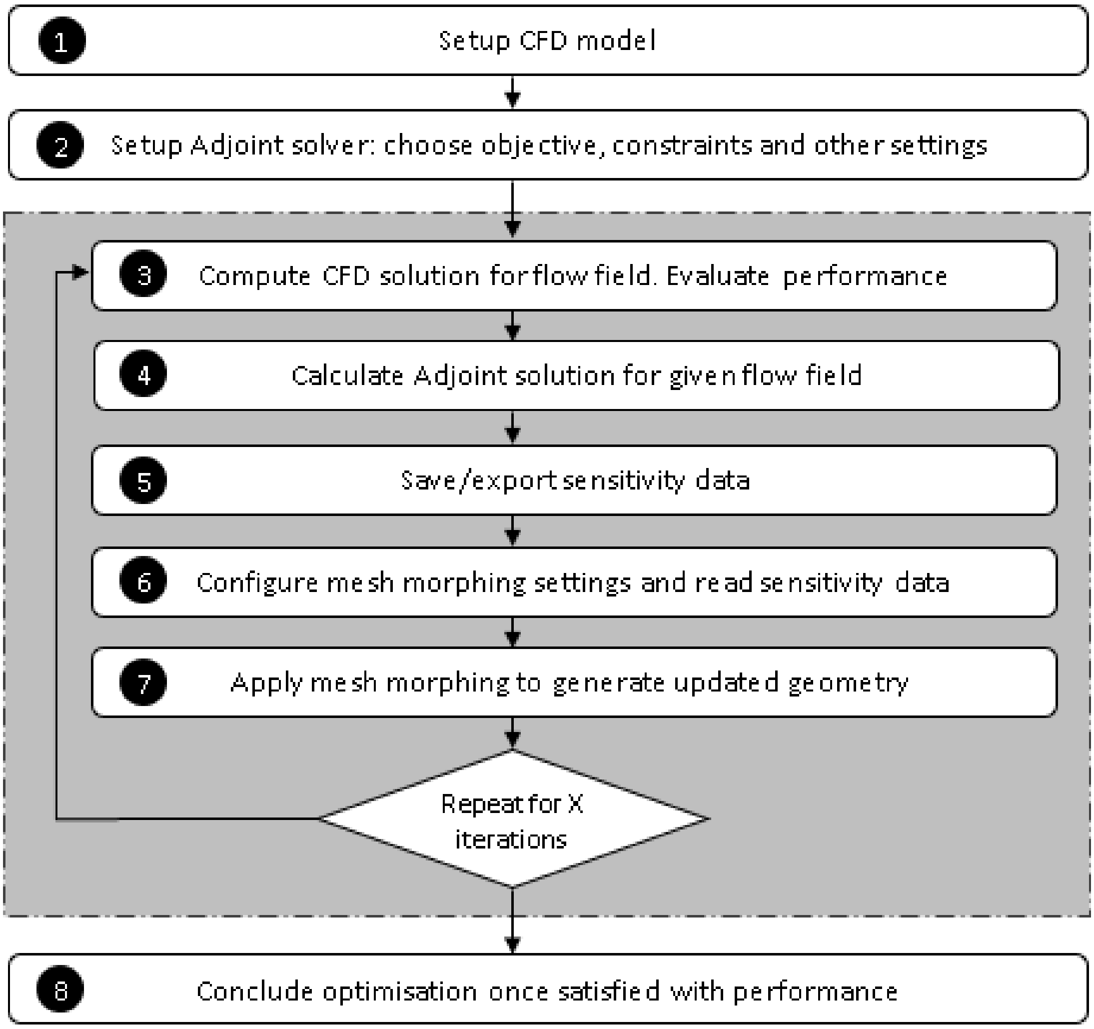

Figure 7 – General Overview of Adjoint Optimisation Procedure

2.4.2 Semi-transient Adjoint Based Optimisation for VAWTs

Figure 8 shows a visual representation of the Adjoint based semi-transient optimisation process in general terms. The goal is to produce a VAWT with an improved average power coefficient compared to the baseline. Graphs of power coefficient C_P are shown for the baseline VAWT (on the left), and for the VAWT with candidate blades (on the right).

As previously described, a Single-Blade model provides an approximate flow field to the VAWT blade. When the blade reaches the snapshot location, the transient

CFD simulation is paused, and an Adjoint solution is taken which generates sensitivity data.

The algorithm produced here is capable of combining the sensitivity data from several snapshots over the cycle. The Adjoint module can then combine these data to produce a single set of sensitivity data that the blade morphing process will use. For illustrative purposes Figure 8 shows three snapshots being used. In the present work however a single snapshot is used per cycle, so no combining of sensitivity data is required (see the planned future work in Section 5).

The mesh morphing tool is then used to update the blade geometry according to the sensitivity data. The new transient flow field is then produced for the updated blade by running further cycles of the CFD model. Several iterations of the Adjoint optimisation process are applied to the Single-Blade model in this fashion which produces an improved blade geometry, referred to as the candidate blade. The candidate blade geometry is then used to produce a VAWT model, so that the VAWT performance improvement can be evaluated. The results of applying the optimisation process to the sample VAWT are shown in Section 3.

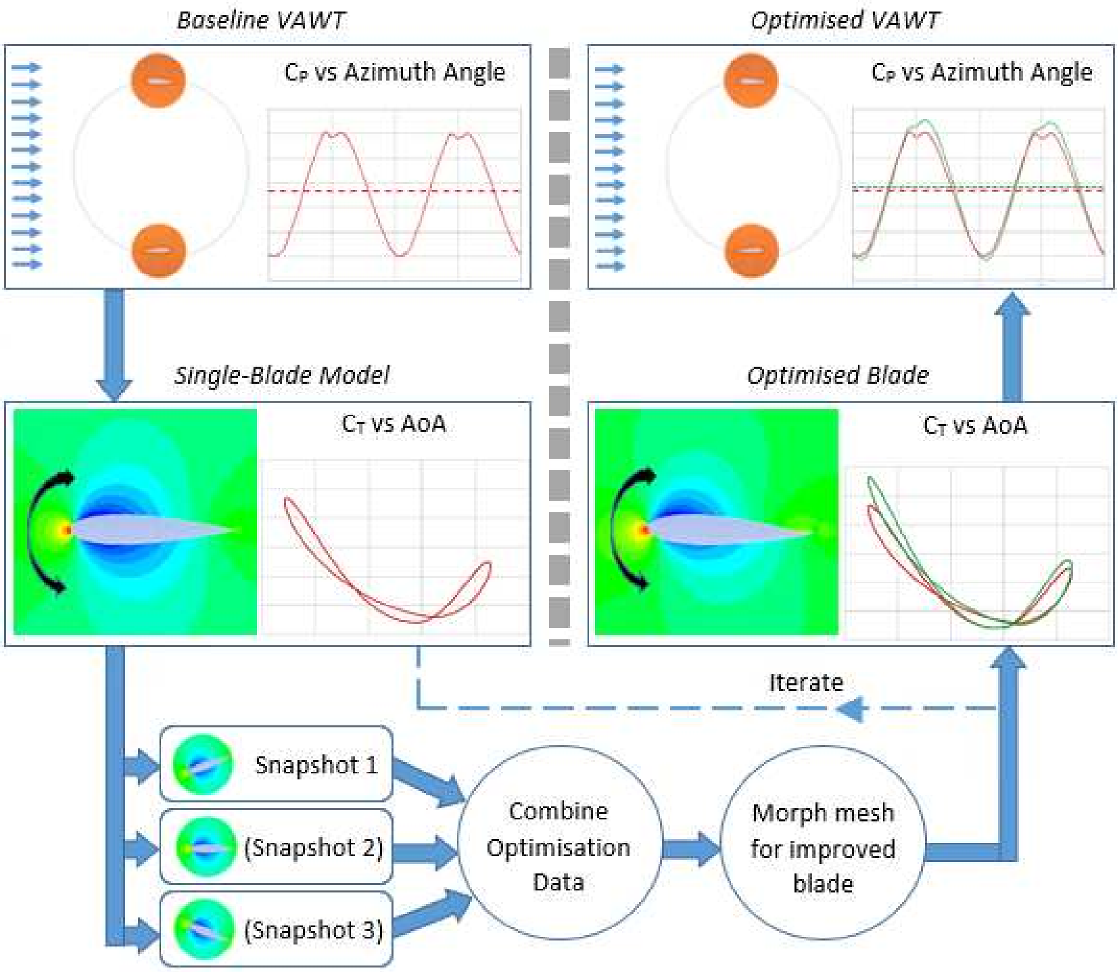

Figure 8 - General Schematic of the Optimisation Process.

2.5 VAWT CFD Models

Once a candidate blade geometry is formed by applying the Single-Blade Adjoint based optimisation process, a VAWT can be constructed to evaluate the blades performance. A VAWT with the baseline blade geometry was also constructed to provide the baseline performance data.

For validation of the baseline VAWT CFD model, independence studies of mesh and time-step were conducted. For the example VAWT of Rezaeiha *et al.* (Vol 107, 2017) used presently, the reference paper contains a thorough domain size study. It is therefore deemed unnecessary for the present works to recount or reconstruct this domain independence study; the final dimensions used here are as recommended by Rezaeiha *et al.* (Vol 107, 2017), and are presented in Table 6.

Dimension	*
dc, Rotating subdomain diameter (as a multiple of turbine diameter)	1.5

di, Distance from turbine centre to inlet (as a multiple of turbine diameter)	10
do, Distance from turbine centre to outlet (as a multiple of turbine diameter)	10
$\frac{1}{2}w$, Half height of domain (from bottom/top boundary to turbine centre)	10

Table 6 - Domain Dimensions (*as a multiple of turbine diameter).

This domain is meshed in a similar way to that described for the Single-Blade model. The same size of near-wall boundary zone is used and the same y+ is achieved. The present mesh independence study therefore uses a range of cases with about 400,000 cells as a medium/fine model (see Table 7).

Mesh I.D.	M1	M2	**M3**	M4	M5
Total cells (k = 1000 cells)	99 k	174 k	**259 k**	461 k	689 k
Num. cells around aerofoil surface	310	380	**475**	570	680

Table 7 – Range of Meshes Used in the Validation Study.

To study the range of meshes, a constant time step of 800 steps/rev was chosen since this was recommended by the Single-Blade validation studies. The coarsest meshes (M1, M2) exhibited a small disagreement with the finer meshes (M3, M4, M5) in the downwind part of the cycle. M3, M4 and M5 shared near perfect agreement demonstrating mesh convergence. The conclusion is therefore that the coarsest mesh in this converged group (M3) is suitable.

The range of time-steps studied are presented in Table 8 and each of them were run with the chosen mesh (M3).

Time Step I.D.	T1	T2	T3	**T4**	T5	T6	T7
Num. steps per turbine revolution	100	200	400	**800**	1200	1600	2000

Table 8 – Range of Time-Steps Used in the Validation Study.

The coarser time steps (T1, T2, and T3) were outliers from the finer time steps (T4, T5, T6 and T7) which showed near perfect agreement with each other. The conclusion is therefore that the time-step T4 (800 time-steps/rev) is suitable.

Figure 9 shows how the baseline blade VAWT CFD model agrees with Rezaeiha *et al.* (Vol 107, 2017). Rezaeiha *et al.* (Vol 107, 2017) also uses 2D simulations but employs the Transition SST turbulence model, which more accurately describes flow transition compared to the k-ω SST model. Therefore some disagreement is found in the downwind part of the cycle, but overall there is good level of agreement which provides confidence in the accuracy of the model used in the present work.

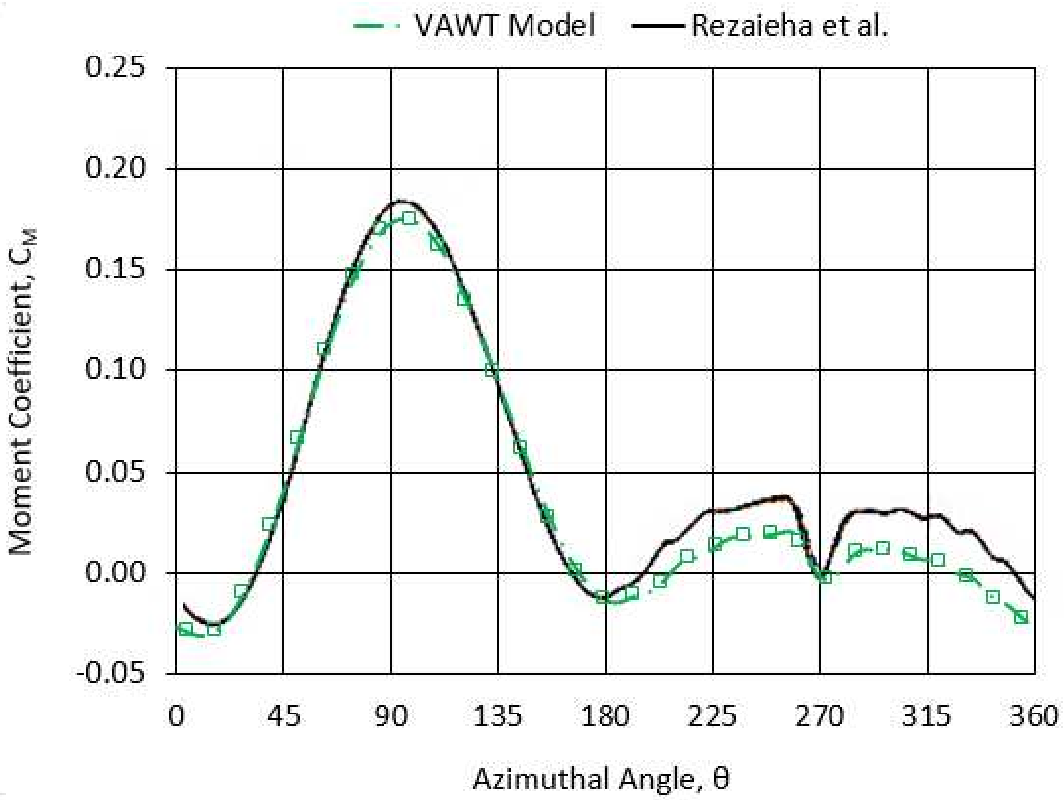

Figure 9 – Baseline VAWT CFD Results and Those Obtained by Rezaeiha *et al.,* (Vol 107, 2017).

The candidate VAWT model is constructed in the same way as the baseline VAWT model described above.

Since the candidate blade geometry in this work is entirely novel, their does not exist any experimental or computational data to validate candidate VAWT data with. Validity of the candidate VAWT model is therefore ensured by its consistency with the validated baseline VAWT model. The candidate VAWT results are shown in Section 3.

3 RESULTS

The investigation of the snapshot location constitutes the cases shown in Table 9. In each case, 10 iterations of the semi-transient Adjoint based optimisation process were conducted, where a single snapshot was taken at the AoA shown in the table. Also provided are the maximum and average increase in C_T achieved by the final candidate blade. Such values are given as a percentage increase relative to the baseline blade. See Figure 11 for example figures illustrating the changes to the C_T curves.

It should be noted that a knockdown factor is applied to the AoA in the downwind part of the cycle. This is achieved via the UDF, as described in Section 2.1. The AoA knockdown is the reason for the lower values of snapshot AoA in the downwind (between 180 and 360 degrees azimuthal position).

Where a negative number occurs for the “max C_T improvement (%)” in Table 9, this tends to indicate that the upwind performance has deteriorated. Such cases tend to show an improvement in the downwind performance.

Case Name /Azimuthal Angle (degrees)	AoA of Snapshot (degrees)	Max C_T improvement	Average C_T Improvement
0	0	-21.3 %	+6.0 %
30	-5.3	-12.5 %	+2.6 %
60	-9.8	+4.9 %	+8.1 %
90	-12.5	+6.9 %	+9.5 %
120	-12.2	+14.6 %	+11.9 %
150	-7.9	+4.5 %	+7.5 %
180	0	-1.1 %	+8.1 %
210	+3.9	-28.6 %	+1.2 %
240	+6.1	-17.7 %	+2.2 %
270	+6.3	-22.3 %	+2.3 %
300	+4.9	-20.1 %	+2.3 %
330	+2.7	-16.4 %	+2.1 %

Table 9 – List of Test Cases and Results after 10 Optimisation Loops are Applied to the Single-Blade Model.

The results of the cases tested in Table 9 can be viewed in greater detail using data of C_T as a function of AoA, along with the aerofoil geometry (see Figure 11 (a) to (c)). This allows visualisation of how the snapshot position corresponds to the blade geometry and performance. This would be too much data to present for each of the 12 cases, so some representative cases are chosen for discussion. Figure 11 (a) shows a typical case with the snapshot located in the upwind region (90° is shown). The results for this case are relatively similar to the others which have snapshot positions between 60°-180°. Such cases are generally characterised by an improvement in the upwind performance, and a relatively unchanged downwind performance. It is noted that the optimised blade geometry shows a toe-out fixing angle and a negative camber. Figure 11 (b) shows a case with the snapshot located at 210° in the downwind region. Such cases show a slight positive camber and improvement in downwind performance, but a reduction in upwind performance. These observations are similar for cases with snapshot located between 210°-330°. Figure 11 (c) shows a case with the snapshot located at 0°. The 0° and 30° cases show a slight negative camber akin to the other upwind cases, but also suffer a reduced upwind performance, and this is possibly due to hysteresis.

To illustrate the role of the Adjoint solution/sensitivity data, Figure 10 shows an example set of sensitivity data for case 90. Figure 10 shows vectors of the shape sensitivity at the 5th (of 10) iteration during the optimisation process. These are directly linked to the resulting geometry shown in Figure 11 (a). The vector arrows indicate the direction for which wall deformation produces an improvement to the objective (C_T). The length of the vector arrows indicates the magnitude of the sensitivity at that location.

Note that there are some large sensitivity vectors that are not shown, which appear at only a few nodes around the geometry. These correspond to inflections in pressure at the leading edge, and the sharp geometry of the trailing edge. The mesh morpher provides smoothing such that these highly sensitive regions do not cause discontinuities in the geometry. It can be observed from Figure 10 that the predominating factor in the shape sensitivity is to raise the leading edge, which manifests as the increased fixing angle and negative camber exhibited in Figure 11 (a).

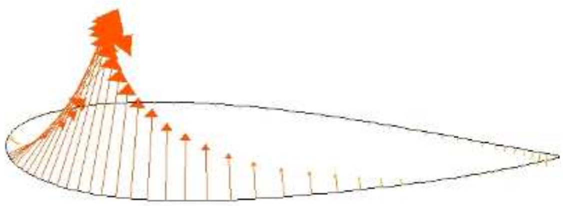

Figure 10 – Vectors of the Shape Sensitivity, Case 90.

(a - snapshot θ = 90°)

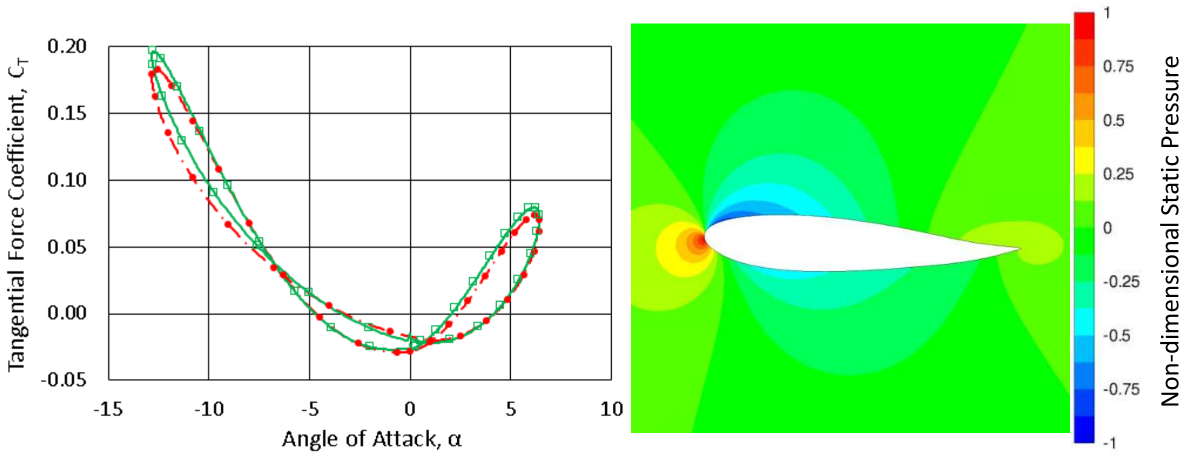

(b - snapshot θ = 210°)

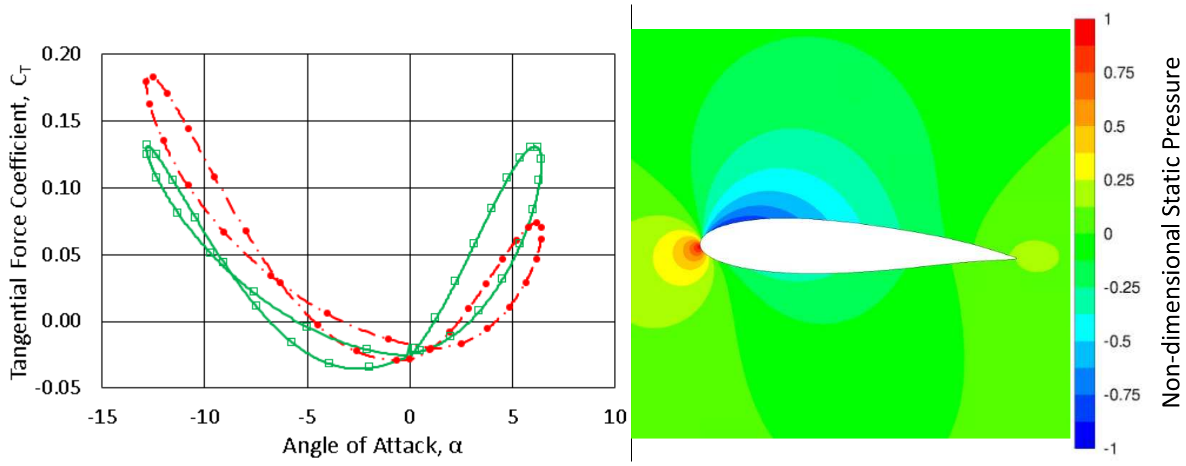

(c - snapshot θ = 0°)

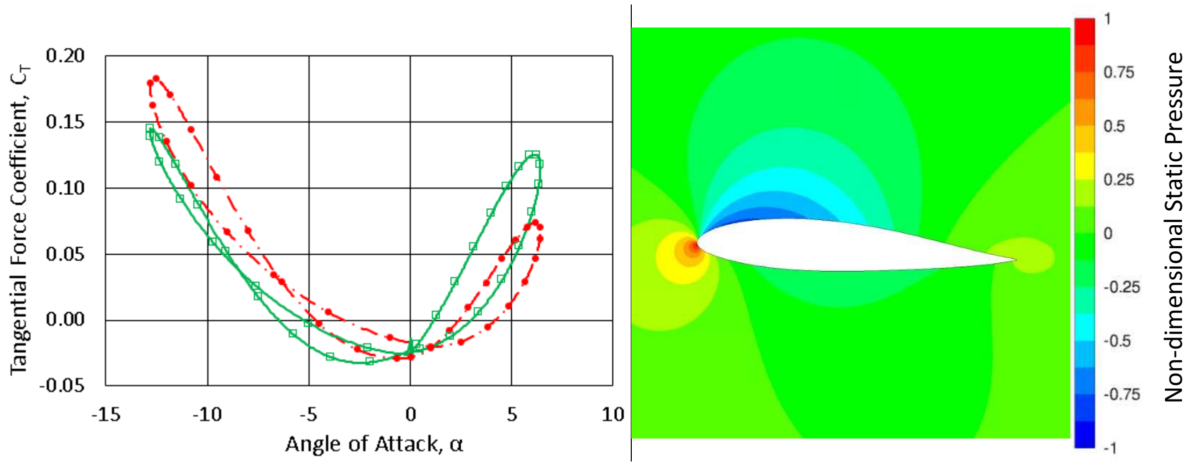

Figure 11 (a) to (c) – 1-Snapshot Investigation Results.

Note: (Left) C_T as a function of AoA - red and green curves represent the baseline and candidate blade performance, respectively. (Right) Candidate blade shape geometries, with contours of the non-dimensional static pressure.

From the results of the Single-Blade model shown in Figure 11 it can be seen that varying levels of performance improvement have been achieved across the cases. The true overall performance is determined by the average C_P which is achieved by the candidate VAWT. As such, the candidate blade geometries were used to construct candidate VAWTs to fully evaluate their performance. Candidate VAWT models are needed because although the Single-Blade model provides a reasonable approximation, it does not accurately reflect the VAWT flow field specifically in the downwind part of the cycle (see Figure 3 and Figure 4). Table 10 summarises the results for these candidate VAWTs accounting for the contribution of both turbine blades and the values are relative to the baseline VAWT.

Case Name /Azimuthal Angle (degrees)	AoA of Snapshot (degrees)	Max VAWT C_M improvement	Average VAWT C_P Improvement
0	0	-5.1 %	+3.5 %
30	-5.3	-3.2 %	+1.4 %
60	-9.8	+2.2 %	+2.4 %
90	-12.5	+2.4 %	+2.1 %
120	-12.2	+6.0 %	+2.3 %
150	-7.9	+1.8 %	+2.2 %
180	0	+0.3 %	+3.0 %
210	+3.9	-7.6 %	+1.5 %
240	+6.1	-4.7 %	+1.3 %
270	+6.3	-5.7 %	+1.3 %
300	+4.9	-5.2 %	+1.3 %
330	+2.7	-4.3 %	+1.3 %

Table 10 – Candidate VAWT, List of Test Cases and Results.

From these results it can be seen that Case 0 produces the greatest improvement to average C_P, of 3.5%. Several simulations were also carried out using the Transition SST model to verify the data from the k-w SST model (Table 10). The 3.5% improvement using the k-w SST model was increased to 5.1% when using the Transition SST model and similar improvements were found in other investigations. Therefore it can be concluded that the encouraging results obtained in Table 10 are a conservative estimate of the improvement that can be obtained

It is also observed that in general, the single snapshot optimisation has resulted in an improvement in the average C_P for all the cases. There is significant variation however on how this is achieved, upwind snapshots tend to improve the upwind performance slightly, and parts of the downwind also remain similar or improve slightly. Downwind snapshots produce a more severe effect on the performance curve, where the downwind performance improves significantly, but the upwind performance deteriorates significantly. Downwind snapshots therefore tend to produce a more even generation of power over the cycle which would offer significantly reduced demand on the electrical generator and lower fatigue loading on the structure.

For discussion/illustration purposes in the remainder of this work, the 90° case will be used. Although case 90 does not provide the greatest improvement, it represents a typical upwind snapshot case. Figure 12 shows the graph of the C_M as a function of the azimuthal angle for a typical upwind snapshot case (case 90), the contribution from only one of the two blades is shown.

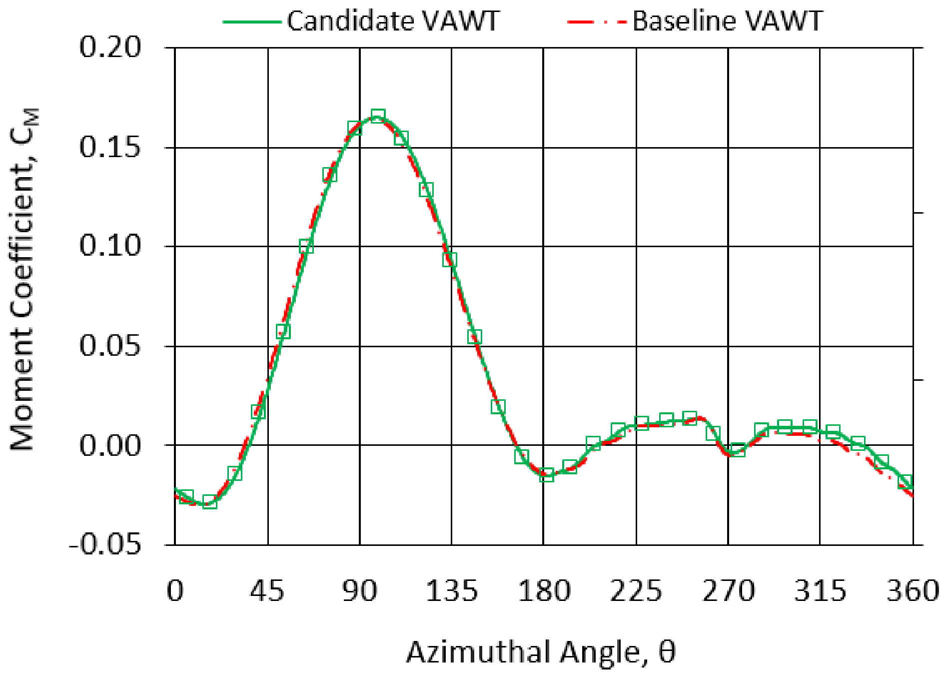

Figure 12 – Candidate VAWT Blade Performance Evaluation (Case 90).

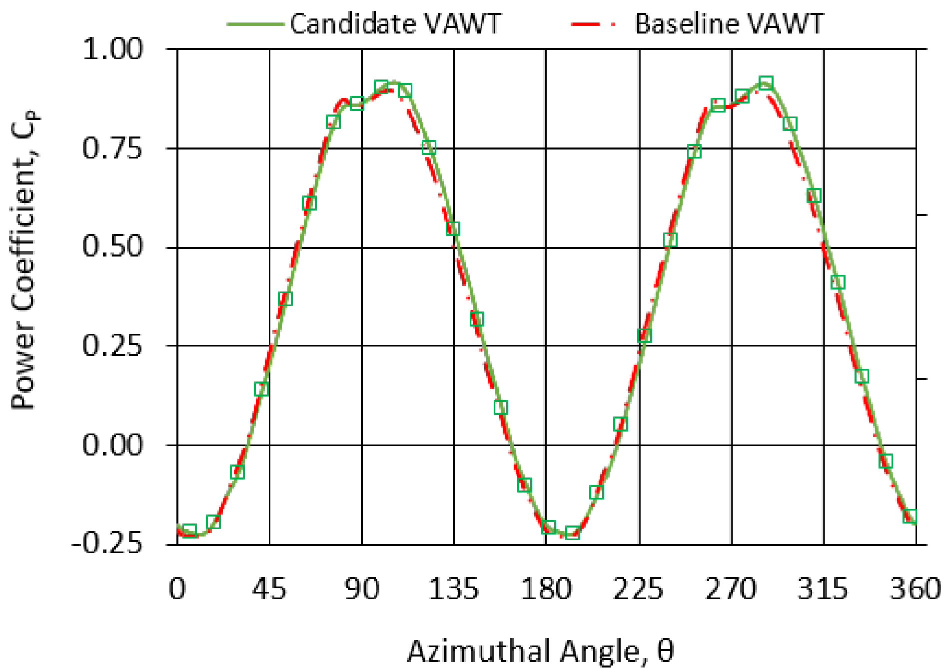

Figure 13 – Candidate VAWT Performance Evaluation (Case 90).

Figure 13 shows the instantaneous power coefficient over one turbine revolution. Note that the power generated is correlated to the moment coefficient, by calculating the total moment of force (contribution of both blades) according to Equation 2.5, and using this value as the torque in Equation 2.6.

A 2.1% improvement to the average C_P was achieved for the typical upwind case (case 90) after 10 iterations of the Adjoint based optimisation process. The candidate blade geometry that produced this improvement is shown in Figure 14 via a static pressure contour plot taken at zero azimuthal angle. Alongside is the baseline (NACA0018) blade geometry for visual comparison. The candidate blade has a toe-out fixing angle of 2°, a maximum camber of 2.0% chord positioned at 80% along the chord (towards the trailing edge), and a maximum thickness of 1% greater than the baseline NACA0018.

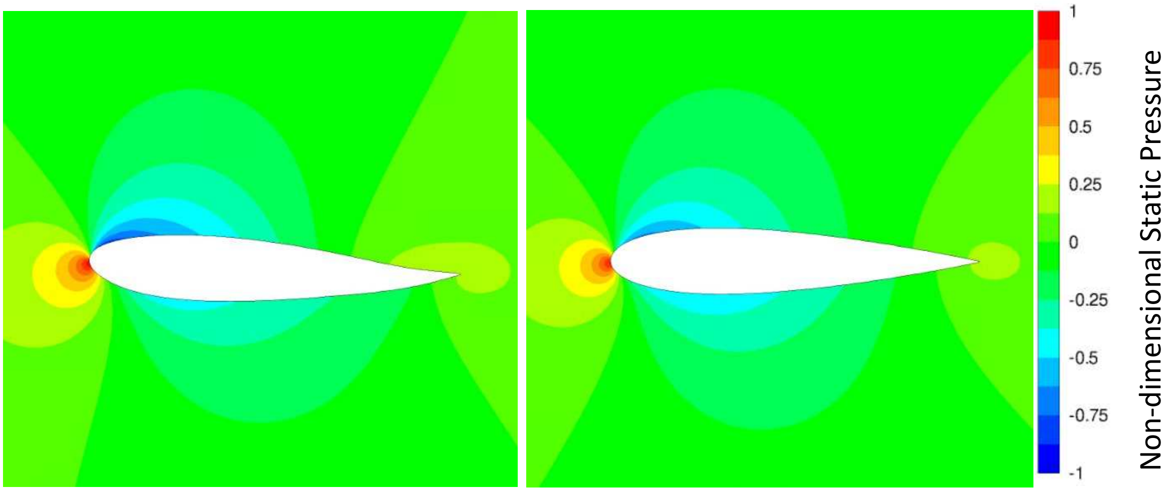

Figure 14 – Blade geometry and contours of the non-dimensional static pressure. (Left) Candidate Blade Case 90, (Right) Baseline Blade.

4 DISCUSSION

The results in Section 3 show that the semi-transient Adjoint based optimisation process applied to a Single-Blade model can be successful. The method shown is in possibly its crudest form using just 1 Adjoint snapshot per cycle, yet after 10 process iterations a candidate blade can be produced that improves the turbine performance. The success of the optimisation process is measured by the average C_P increase of the candidate VAWT. The following are some general observations from the range of results:

- After applying the semi-transient optimisation process to the Single-Blade model, the performance curve (C_T as a function of AoA) is improved in the region around the location at which the snapshot is taken.
- All cases have resulted in improvement to VAWT average C_P.
- When the Single-Blade model predicts a large max C_T increase in the upwind part of the cycle, this also translates to a max C_P increase in the candidate VAWT model, although not of the same magnitude.
- The *average* C_T improvements seen in the Single-Blade model do *not* translate to similar improvements in the *average* C_P in the VAWT model. This is due to the inaccuracies in the downwind flow field that the Single-Blade model provides (see Figure 3).
- A negative camber is correlated with improvements to the upwind part of the cycle, and a positive camber to the downwind part.
- Upwind snapshot cases tend to increase the moment coefficient over the majority of the revolution but only by a small amount.
- Downwind snapshot cases tend to improve the moment coefficient in the downwind, reduce it in the upwind, and generally provide a smoother power curve that also has a slight average C_P improvement.

The candidate blade geometry has a negative (toe-out) fixing angle of around 2°. A maximum negative camber of around 2% is also present, located at around 80% chord length. The candidate blade is 1% thinner than the baseline NACA0018.

Figure 15, shows the streamlines (coloured by static pressure) over the candidate blade and baseline blade when at 90° azimuthal angle. Figure 16 shows the corresponding surface pressure coefficients. The surface pressures of the candidate blade exhibit a weaker negative pressure on the suction side of the blade at the leading edge. The candidate blades increased fixing angle means that less curvature is demanded from the flow to pass around the leading edge, and while this reduces leading edge suction it allows a greater suction to be maintained along the mid-chord and towards the trailing edge. Towards the aft of the blade the magnitude of positive pressure on the top surface is also increased due to the introduced camber. At the trailing edge where the camber is most pronounced, a high pressure zone can be observed on the top surface of the candidate blade. This is coupled with a greater suction also towards the trailing edge, such that a more favourable magnitude and direction of pressure gradient is achieved compared to the baseline blade. At this location the trailing edge geometry slightly changes the size and shape of the small recirculating region but this has only minimal effect on the surface pressures.

Figure 17 shows streamlines (coloured by static pressure), and Figure 18 shows surface pressures for the position of 270° azimuthal angle. The surface pressures of the candidate blade exhibit a higher suction peak on the top surface of the blade at the leading edge. This is due to the fixing angle of the candidate blade; at this point in the revolution the fixing angle demands more curvature from the flow around the LE. The camber effect produces higher pressure gradients compared to the baseline blade, moving from the mid-chord towards the trailing edge. The large suction and pressure region located at 0.8 chord (Figure 18) corresponds to the position of maximum camber.

The candidate blade geometry is therefore aerodynamically advantageous over the majority of the turbine cycle, producing a greater average C_P compared to the VAWT with baseline (NACA0018) blades.

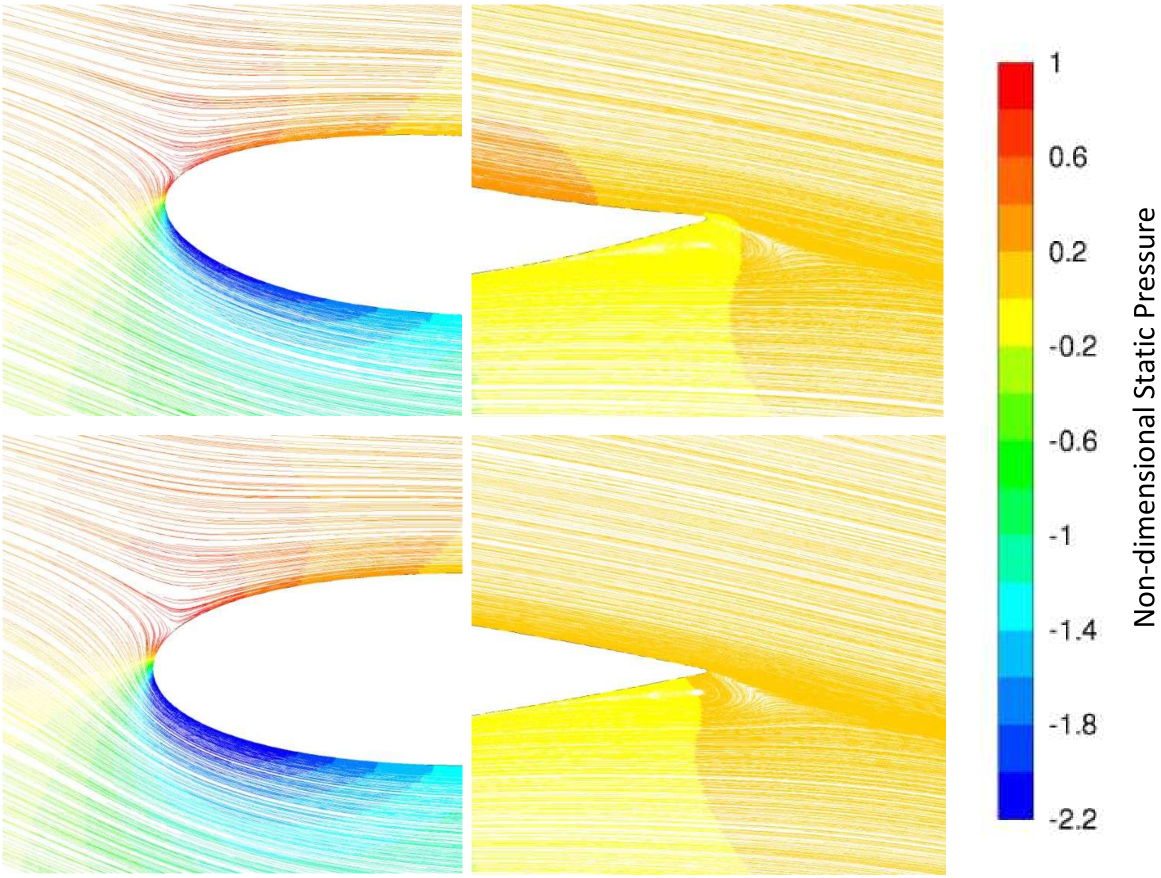

Figure 15 - VAWT blade streamlines (coloured by the non-dimensional static pressure) at 90° azimuthal angle. (Top) Candidate blade from Case 90. (Bottom) Baseline blade).

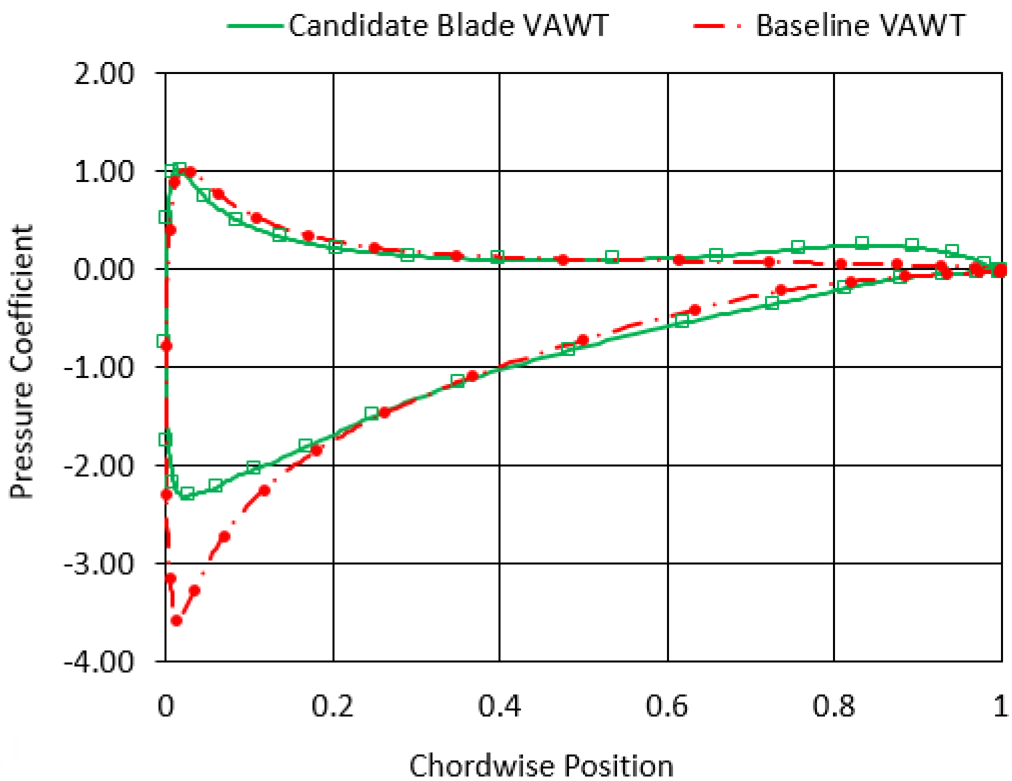

Figure 16 - VAWT blade surface pressure coefficient at 90° azimuthal angle.

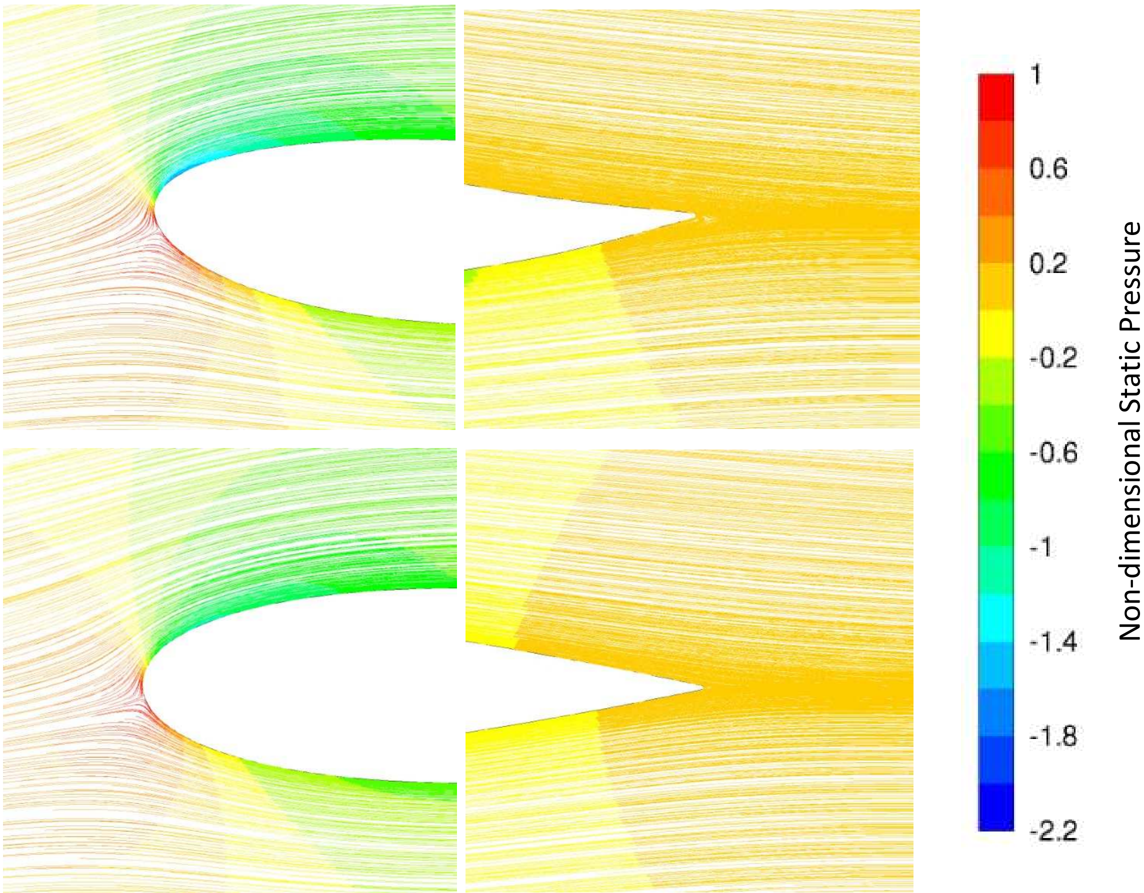

Figure 17 - VAWT blade streamlines (coloured by the non-dimensional static pressure) at 270° azimuthal angle. (Top) Candidate blade from Case 90. (Bottom) Baseline blade).

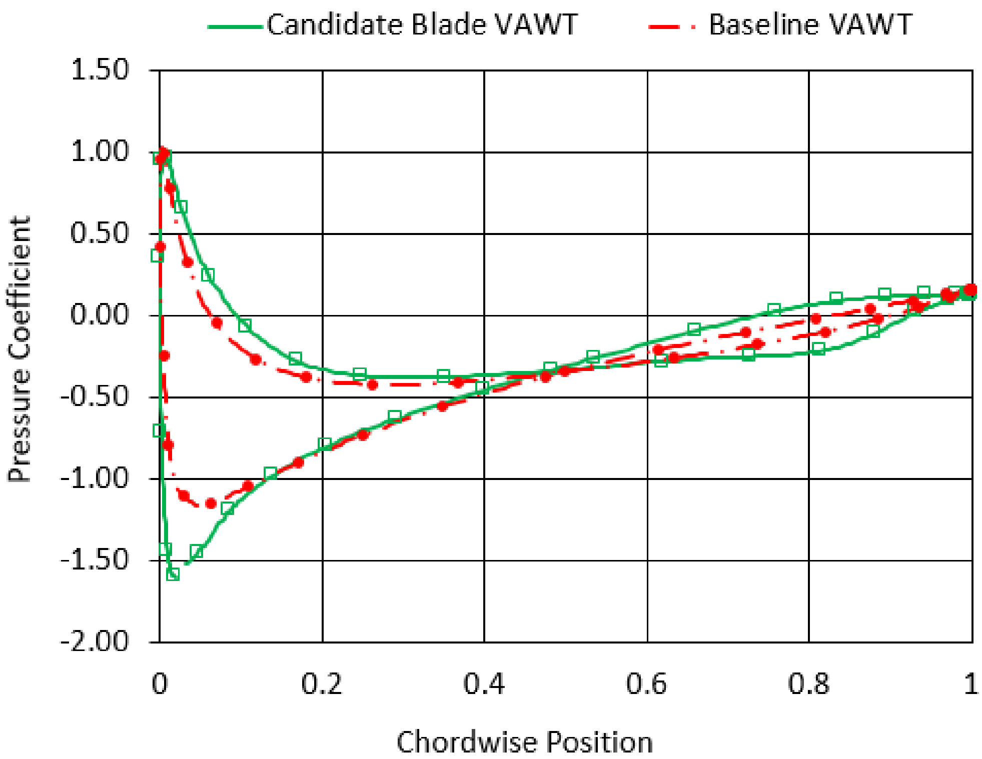

Figure 18 - VAWT blade surface pressure coefficient at 270° azimuthal angle.

The presented results are significant because they demonstrate the successful application of Adjoint methods to VAWTs, using commercial CFD software and a promising semi-transient optimisation process. The method presented is in a fundamental/basic form using just 1 Adjoint snapshot per revolution for the optimisation. This leaves great scope for development of these methods and further improvement to VAWT performance. In addition, the discussion has explored a novel VAWT blade geometry, and the associated links to performance characteristics and improvement. Also it should be noted that the case illustrated in this paper is for a high TSR (4.5) turbine and that sensitivity data from the downwind part of the cycle is not considered; the method may require further development for compatibility with low TSR cases that carry greater levels of flow unsteadiness.

5 CONCLUSION

This paper set out to apply powerful Adjoint methods to the problem of VAWT aerodynamics to produce a low-cost optimisation process. In the absence of literature on this topic, a semi-transient Adjoint based optimisation process was developed which was limited to use just 1 Adjoint solution (or 'snapshot') per turbine revolution to demonstrate its feasibility.

The optimisation process was applied to a typical turbine with a TSR of 4.5, and a range of permutations of the method were tested. The results demonstrate that a steady Adjoint solver incorporating unsteady CFD simulations can successfully optimise VAWT blade geometry using just 1 Adjoint snapshot per revolution. Furthermore, an approximation model with a single, pitching blade can be used during the optimisation process to approximate the VAWT flow field whilst reducing computation cost.

This paper demonstrates the viability of the method using the ANSYS Fluent CFD code, but the method can be implemented in alternative codes which have an Adjoint solver. A Single-Blade approximation model is used which provides sufficient flow field accuracy for Adjoint solutions to be taken in the upwind region, but poor accuracy in the downwind. Furthermore, CFD analysis is conducted using the SST k-ω turbulence model throughout rather than a more accurate approach such as LES. The modelling uncertainty can therefore be not insignificant but is aligned with much of the existing literature where low computation cost is needed. Despite the modelling assumptions, the effectiveness of the semi-transient Adjoint optimisation method has been shown. Furthermore, the method even in a basic formulation has shown positive results where VAWT performance can be quickly improved. This is therefore a promising avenue of research and it is envisaged that improved results could be seen when possible areas of refinement are explored. It is likely that a substantially improved, and more generalised optimisation process can be developed in future. The combining of multiple snapshots over each cycle could provide a blade that performs better over a range of azimuthal angles, thereby improving the average power coefficient. Improvements could be made to the Single-Blade approximation model such that it more closely reproduces the VAWT flow field. A range of turbines and operating conditions could be examined, in order to inform a generalised approach for choosing the appropriate number/location of snapshots to use for optimising a new VAWT. The CFD modelling, specifically of the candidate VAWT models could be refined by using more advanced turbulence models to give better accuracy in predicting VAWT performance. The method could also be extended to 3D simulations, which could offer turbine blades optimised with spanwise geometry variations.

ACKNOWLEDGEMENT

The authors would like to express gratitude to the Engineering and Physical Sciences Research Council (EPSRC) for financially supporting this work.

6 APPENDIX A – UDF FOR SINGLE BLADE MODEL

The UDF used to provide the oscillation profile and variable inlet velocity profile is shown here. Note that ANSYS Fluent requires the AoA profile to be specified as a function of rotational velocity, omega.

```
#include "udf.h"
#define TSR 4.5      /* constants , tip speed ratio*/
#define velocity_free 9.3  /*free flow velocity*/
#define thetamax 0.22393
#define w 83.7

DEFINE_TRANSIENT_PROFILE(angular_velocity,time)
{
  real omega, theta;
  theta = (w*time) - 6.283185307*floor((w*time)/6.283185307);
  if (theta > 3.141592654 && theta < 6.283185307)
  omega =0.5*w*(1+TSR*cos(w*time))/(1+2*TSR*cos(w*time)+(TSR*TSR));
  else
  omega =w*(1+TSR*cos(w*time))/(1+2*TSR*cos(w*time)+(TSR*TSR));
  return omega;
}

DEFINE_PROFILE(unsteady_velocity, thread, position)
{
  face_t f;
  real t = CURRENT_TIME;
  real theta = w*t;
  real alpha = atan(sin(theta)/(TSR+cos(theta)));
  begin_f_loop(f, thread)
    {
      F_PROFILE(f, thread, position) =
velocity_free*sqrt(1+pow(TSR,2)+2*TSR*cos(theta));
    }
  end_f_loop(f, thread)
}
```

7 REFERENCES

ANSYS Inc. ANSYS Help, Release 18.2. (2017).

ANSYS Inc. Introduction to ANSYS Fluent, Module 07: Turbulence. Release 17.0. (2016).

Ashwill, T. D. Measured Data for the Sandia 34-Meter Vertical Axis Wind Turbines, SAND91-2228, Sandia Corporation. (1992).

Almohammadi, K. M., Ingham, D. B., Ma, L. & Pourkashanian, M. 2D CFD Analysis of the Effect of Trailing Edge Shape on the Performance of a Straight-Blade Vertical Axis Wind Turbine. IEEE Transactions on Sustainable Energy Vol 6. (2015), pp. 228-235.

Baker, J. R. Features to aid or enable self starting of fixed pitch low solidity vertical axis wind turbines. Journal of Wind Engineering and Industrial Aerodynamics Vol 15. (1983), pp. 369-380.

Balduzzi, F., Bianchini, A., Maleci, R., Ferrara, G. & Ferrari, L. Critical issues in the CFD simulation of Darrieus wind turbines. Renewable Energy Vol 85. (2015), pp. 419-435.

Bianchini, A., Ferrara, G. & Ferrari, L. Design guidelines for H-Darrieus wind turbines: Optimization of the annual energy yield. Energy Conversion and Management Vol 89. (2014), pp. 690-707.

Bhutta, M. M. A., Hayat, N., Farooq, U.H., Ali, Z., Jamil, S.R. & Hussain, Z. et al. Vertical axis wind turbine – A review of various configurations and design techniques. Renewable and Sustainable Energy Reviews Vol 16. (2011), pp. 1926-1939.

Carpentieri, G. PhD Thesis: An Adjoint-Based Shape-Optimization Method for Aerodynamic Design. Delft University of Technology. (2009).

Coppin, J. PhD Thesis: Aerodynamics, Stability and Shape Optimisation of Unmanned Combat Air Vehicles. University of Sheffield. (2014).

Coton, F. N., Galbraith, R. A. M. & Jiang, D. The Influence of Detailed Blade Design on the Aerodynamic Performance of Straight-Bladed Vertical Axis Wind Turbines. IMechE Part A: Power and Energy Vol 210. (1996), pp. 65-74.

Daróczy, L., Janiga, G. & Thévenin, D. Computational fluid dynamics based shape optimization of airfoil geometry for an H-rotor using a genetic algorithm. Engineering Optimization, (2018), pp. 1-17.

Dhert, T., Ashuri, T. & Martins, J. Aerodynamic shape optimization of wind turbine blades using a Reynolds-averaged Navier–Stokes model and an adjoint method. Wind Energy Vol 20. (2016), pp. 909-926.

Edwards, J. M. PhD Thesis: The influence of aerodynamic stall on the performance of vertical axis wind turbines. University of Sheffield. (2012).

Eggenspieler, G. Product Presentation: ANSYS Fluent Adjoint Solver. ANSYS Inc. (2012).

Errico, R. M. What is an adjoint model? Bulletin of the American Meteorological Society Vol 78. (1997), pp. 2577-2591.

Ferrer, E. & Montlaur, A. CFD for Wind and Tidal Offshore Turbines. Springer. (2015).

Funke, S. W., Farrell, P. E. & Piggott, M. D. Tidal turbine array optimisation using the Adjoint approach. Renewable Energy Vol 63. (2013), pp. 658-673.

Gosselin, R., Dumas, G. & Boudreau, M. Parametric study of H-Darrieus vertical-axis turbines using uRANS simulations. Conference of the CFD Society of Canada #178 Session 13-6 (2013), pp. 1-16.

Guo, Y., Li, X., Sun, L., Gao, Ye., Gao, Z. & Chen, L. Aerodynamic analysis of a step adjustment method for blade pitch of a VAWT. Journal of Wind Engineering & Industrial Aerodynamics Vol 188. (2019), pp. 90-101.

Hand, B., Kelly, G. & Cashman, A. Numerical simulation of a vertical axis wind turbine airfoil experiencing dynamic stall at high Reynolds numbers. Computers & Fluids Vol 149. (2017), pp. 12-30.

Hill, N., Dominy, R., Ingram, G. & Dominy, J. Darrieus turbines: The physics of self-starting. IMechE Part A: Power and Energy Vol 223. (2008), pp. 21-29.

Howell, R., Qin, N., Edwards, J. & Durrani, N. Wind tunnel and numerical study of a small vertical axis wind turbine. Renewable Energy Vol 35. (2009), pp. 412-422.

Islam, M., Ting, D. S. & Fartaj, A. Desirable Airfoil Features for Smaller-Capacity Straight-Bladed VAWT. Wind Engineering Vol 31. (2007), pp. 165-196.

Jin, X., Zhao, G., Gao, K. & Ju, W. Darrieus vertical axis wind turbine: Basic research methods. Renewable and Sustainable Energy Reviews Vol 42. (2014), pp. 212-225.

Klimas, P. C. & Worstell, M. H. Effects of Blade Preset Pitch/ Offset on Curved-Blade Darrieus Vertical Axis Wind Turbine Performance, SAND-81-1762. Sandia Corporation. (1981).

Le Moigne, A. PhD Thesis: A Discrete Navier-Stokes Adjoint Method for Aerodynamic Optimisation of Blended Wing-Body Configurations. University of Sheffield. (2003).

Li, H., Song, L., Li, Y. & Feng, Z. 2D Viscous Aerodynamic Shape Design Optimization for Turbine Blades Based on Adjoint Method. Journal of Turbomachinery Vol 133. (2011), pp. (031014)1-8.

Li, C., Xiao, Y., Xu, Y-L., Peng, Y-X., Hu, G. & Zhu, S. Optimization of blade pitch in H-rotor vertical axis wind turbines through computation fluid dynamics simulations. Applied Energy Vol 212. (2018), pp. 1107-1125.

Luo, J., Xiong, J., Liu, F. & McBean, I. Three-Dimensional Aerodynamic Design Optimization of a Turbine Blade by Using an Adjoint Method. Journal of Turbomachinery Vol 133. (2011), pp. (011026)1-11.

Peter, J. E. V. & Dwight, R. P. Numerical sensitivity analysis for aerodynamic optimization: A survey of approaches. Computers & Fluids Vol 39. (2010), pp. 373-391.

Rezaeiha, A., Kalkman, I., Blocken, B. CFD simulation of a vertical axis wind turbine operating at a moderate tip speed ratio: Guidelines for minimum domain size and azimuthal increment. Renewable Energy Vol 107. (2017), pp. 373-385.

Rezaeiha, A., Kalkman, I., Blocken, B. Effect of pitch angle on power performance and aerodynamics of a vertical axis wind turbine. Applied Energy Vol 197. (2017), pp. 132-150.

Rezaeiha, A., Montazeri, H., Blocken, B. Towards accurate CFD simulations of vertical axis wind turbines at different tip speed ratios and solidities: Guidelines for azimuthal increment, domain size and convergence. Energy Conversion and Management Vol 156. (2018), pp. 301-316.

Rezaeiha, A., Montazeri, H., Blocken, B. On the accuracy of turbulence models for CFD simulations of vertical axis wind turbines. Energy Vol 180. (2019), pp. 838-857.

Sutherland, H. J., Berg, D. E. & Ashwill, T. D. A Retrospective of VAWT Technology, SAND-2012-0304, Sandia Corporation. (2012).

Tescione, G., Ragni, D., He, C., Simao, C.J. & van Bussel, G.J.W. Near wake flow analysis of a vertical axis wind turbine by stereoscopic particle image velocimetry. Renewable Energy Vol 70. (2014), pp. 47-61.

Tjiu, W., Marnoto, T., Mat, T., Ruslan, M. H. & Sopian, K. Darrieus vertical axis wind turbine for power generation I: Assessment of Darrieus VAWT configurations. Renewable Energy Vol 75. (2014), pp. 50-67.

Walther, B. & Nadarajah, S. An Adjoint-Based Multi-Point Optimization Method for Robust Turbomachinery Design. ASME Turbo Expo 2015, GT2015-44142. (2015), pp. 1-12.

Wang, S., Ingham, D. B., Ma, L., Pourkashanian, M. & Tao, Z. Numerical investigations on dynamic stall of low Reynolds number flow around oscillating airfoils. Computers & Fluids Vol 39. (2010), pp. 1529-1541.

Worasinchai, S., Ingram, G. L. & Dominy, R. G. The Physics of H-Darrieus Turbine Starting Behavior. Journal of Engineering for Gas Turbines and Power Vol 138. (2016), pp. (062605)1-11.

Worstell, M. H. Aerodynamic Performance of the 17 Meter Diameter Darrieus Wind Turbine, SAND78-1737, Sandia Corporation. (1978).

Vassberg, J. C., Gopinath, A. K. & Jameson, A. Revisiting the Vertical-Axis Wind-Turbine Design using Advanced Computational Fluid Dynamics. AIAA ASM Vol 43. (2005), pp. 1-23.

Zhang, T-T., Elsakka, M., Huang, W., Wang, Z-G., Ingham, D. B,, Ma, L. & Pourkashanian, M. Winglet design for vertical axis wind turbines based on a design of experiment and CFD approach. Energy Conversion and Management Vol 195. (2019), pp. 712-726.

Zhu, J., Huang, H. & Shen, H. Self-starting aerodynamics analysis of vertical axis wind turbine. Advances in Mechanical Engineering Vol 7. (2015), pp. 1-12.